

Nuclear energy density functionals from machine learning

X. H. Wu (吴鑫辉),¹ Z. X. Ren (任政学),¹ and P. W. Zhao (赵鹏巍)^{1,*}

¹*State Key Laboratory of Nuclear Physics and Technology,
School of Physics, Peking University, Beijing 100871, China*

Abstract

Machine learning is employed to build an energy density functional for self-bound nuclear systems for the first time. By learning the kinetic energy as a functional of the nucleon density alone, a robust and accurate orbital-free density functional for nuclei is established. Self-consistent calculations that bypass the Kohn-Sham equations provide the ground-state densities, total energies, and root-mean-square radii with a high accuracy in comparison with the Kohn-Sham solutions. No existing orbital-free density functional theory comes close to this performance for nuclei. Therefore, it provides a new promising way for future developments of nuclear energy density functionals for the whole nuclear chart.

Research on quantum mechanical many-body problems is essential in a wide variety of scientific fields. By reducing the many-body problem formulated in terms of N -body wave functions to the one-body level with the density distributions, the density functional theory (DFT) has been enormously popular. However, the quality of the DFT results crucially depends on the accuracy of the energy density functional, whose existence was proved by the Hohenberg-Kohn theorem [1], but the actual form is unknown and has to be determined with approximations.

Kohn and Sham first made DFT into a practical tool by computing the exact kinetic energy of an interacting many-body system with a noninteracting single determinantal wave function that gives rise to the same density [2]. Since the kinetic energy is a major unknown part of the energy density functionals, the Kohn-Sham DFT is remarkably accurate [3]. Nevertheless, this approach involves not only the density but also the auxiliary one-body orbitals which need to be obtained by solving the so-called Kohn-Sham equation self-consistently. This leads to enormous amount of work, in particular for systems with a large number of particles.

On the other hand, one of the aims of DFT is to express the energy solely as a functional of the density, i.e., orbital-free DFT. It is directly based on the Hohenberg-Kohn theorem [1], and is much more efficient than Kohn-Sham DFT due to the avoidance of the auxiliary one-body orbitals. However, it brings an inevitable trade-off between efficiency and accuracy. Instead of using orbitals to compute the kinetic energy, orbital-free DFT uses approximate kinetic energy density functionals, e.g., the well-known Thomas-Fermi functionals [4], which renders it less accurate than Kohn-Sham DFT in most cases. Therefore, an accurate and computationally efficient orbital-free DFT is highly desired.

Of course, the stumbling block is that, as yet, no sufficiently accurate descriptions of kinetic energy with the density alone has been found. Despite more than seventy years of research and some tremendous progress, it is still a bottleneck of the DFT computations in various scientific fields. For nuclear physics, it is even more elusive because of the complicated short-range two nucleon interactions. In fact, for a local Skyrme energy density functional, the Thomas-Fermi solution of the ground-state density gives no spatial dependence whatsoever [5]. The description could be improved with higher-order corrections in the \hbar expansion of the kinetic energy. However, there are still obvious deviations from the Kohn-Sham energy for the Thomas-Fermi approximation even corrected up to the \hbar^4 or-

der due to the missing of sufficient quantum effects [6]. As a result, most modern DFT calculations in nuclear physics are based on the Kohn-Sham approach [7–10].

The recent rise in the popularity of machine learning (ML) has engendered many advances in various fields [11, 12]. Machine learning is a powerful tool for finding patterns in high-dimensional data, so it holds the promise of learning the energy density functional from sufficient “energy-density data” via induction. While applications of ML approaches to DFTs in condensed-matter physics and quantum chemistry have been proliferating in the past few years, the adoption in realistic computations is still in its infancy [13–15]. For nuclear physics, ML applications can be traced back to early 1990s [16, 17], and recently, it has been more broadly adopted to nuclear masses [18–22], charge radii [23–25], excited states [26], fission yields [27], variational calculations [28], etc. However, the application of ML to develop density functionals for nuclear systems is still a blank area.

In contrast to the many-electron systems trapped in an external field in condensed-matter physics and quantum chemistry, nuclei are self-bound via strong and short-range nucleon-nucleon interactions. Thus, the nuclear DFTs are formulated in terms of the so-called “intrinsic” one-body density [10] (e.g., the density relative to the center-of mass). While ML is a balanced interpolation on known data and should be unreliable for densities far from the training set, fortunately, due to the saturation of nuclear forces, the intrinsic nucleon density is of size similarity for nuclei with different numbers of nucleons. This property is useful to simplify the ML model and/or reduce the demands of a huge training data set.

In this Letter, for the first time, ML is used to build an energy density functional for nuclei. The employed ML model is kernel ridge regression (KRR) [29, 30], which is trained to describe the kinetic energy with the nucleon density alone. An orbital-free density functional for nuclei is thus established after including the interaction energy. As the first attempt, self-consistent calculations that bypass the Kohn-Sham equation are carried out for three nuclei ${}^4\text{He}$, ${}^{16}\text{O}$, and ${}^{40}\text{Ca}$, and they illustrate the key issues for applying ML to nuclear DFT problems.

The nuclear DFT starts from an energy density functional

$$E_{\text{tot}}[\rho(\mathbf{r})] = E_{\text{kin}}[\rho(\mathbf{r})] + E_{\text{int}}[\rho(\mathbf{r})], \quad (1)$$

which consists of the kinetic and interaction energies. The interaction energy is obtained by assuming the nucleon-nucleon effective interaction, for simplicity, as a local Skyrme interac-

tion [31],

$$E_{\text{int}}[\rho(\mathbf{r})] = \int \left(-\frac{1}{2}a\rho^2 + \frac{1}{3}b\rho^3 \right) d^3\mathbf{r}, \quad (2)$$

where $a = 817.5 \text{ MeV}\cdot\text{fm}^3$ and $b = 3241.5 \text{ MeV}\cdot\text{fm}^6$ are two coupling constants. The nonlocal terms in the Skyrme interaction are neglected, but their contributions are relatively small and can be considered straightforwardly [5].

In contrast to the Kohn-Sham approach, the kinetic energy here is expressed solely as a functional of the density with the KRR approach [29, 30], which is a powerful machine-learning approach for nonlinear regression,

$$E_{\text{kin}}^{\text{ML}}[\rho(\mathbf{r})] = \sum_{i=1}^m \omega_i K(\rho_i, \rho). \quad (3)$$

Here, ω_i are weights to be determined, $\rho_i(\mathbf{r})$ are training densities, and K is the kernel function, which measures the similarity between densities,

$$K(\rho, \rho') = \exp \left[-\|\rho(\mathbf{r}) - \rho'(\mathbf{r})\|^2 / (2AA'\sigma^2) \right]. \quad (4)$$

Here, σ is a hyperparameter defining the length scale on the distance that the kernel affects, and the distance between two densities $\|\rho(\mathbf{r}) - \rho'(\mathbf{r})\|$ can be calculated by vectorizing the densities on a series of discrete grids. The factors A and A' are the nucleon numbers of the densities ρ and ρ' , respectively. They are introduced to scale the density distance, so that the kernel function K can be directly applied to densities with different nucleon numbers. This is important for applying the present ML approach to the whole chart of nuclei in the future.

The weights w_i are determined by minimizing the loss function defined as

$$L(\boldsymbol{\omega}) = \sum_{i=1}^m (E_{\text{kin}}^{\text{ML}}[\rho_i] - E_{\text{kin}}[\rho_i])^2 + \lambda \|\boldsymbol{\omega}\|^2, \quad (5)$$

where $\boldsymbol{\omega} = (w_1, \dots, w_m)$. The first term is quadratic sum of the differences between the exact kinetic energy E_{kin} and the ML predictions $E_{\text{kin}}^{\text{ML}}$ for each density ρ_i . The second term with the hyperparameter λ is a regularizer that penalizes large weights to reduce the risk of overfitting. Minimizing the loss function yields

$$\boldsymbol{\omega} = (\mathbf{K} + \lambda \mathbf{I})^{-1} \mathbf{E}_{\text{kin}}, \quad (6)$$

where \mathbf{K} is the kernel matrix with elements $\mathbf{K}_{ij} = K(\rho_i, \rho_j)$, \mathbf{I} is the identity matrix, and \mathbf{E}_{kin} are the exact kinetic energies to be learned, i.e., $(E_{\text{kin}}[\rho_1], \dots, E_{\text{kin}}[\rho_m])$.

The nuclear ground state is obtained by a variation of the energy density functional with respect to the density. The variation of the interaction energy (2) can be readily obtained, while for the kinetic energy, it reads

$$\frac{\delta E_{\text{kin}}^{\text{ML}}[\rho]}{\delta \rho} = \sum_{i=1}^m \frac{w_i}{AA_i\sigma^2}(\rho_i - \rho)K(\rho_i, \rho). \quad (7)$$

This functional derivative follows again a weighted summation of the kernel functions with the weights related to deviations from the training densities ($\rho_i - \rho$). However, this would cause huge errors in the functional derivative because Eq. (7) does not contain information on how the energies change along all directions, but only directions in which it has training data. There have been various ways to overcome this problem in the literature, see e.g., Refs [14, 32]. Here, we employ a prime local principal component analysis [32, 33] to calculate the functional derivative, and the accuracy is found to be rather good for nuclei. Once the functional derivative is obtained, the self-consistent ground-state density can be calculated with the gradient descent method starting from a trial density.

Without loss of generality, in this work, we only consider spherical nuclei with the same proton and neutron numbers. The densities to be learned by the KRR network can be reduced to the one-dimensional radial densities with the metric $\tilde{\rho}(r) = 4\pi r^2 \rho(r)$, and they are expressed in 501 discretized spatial mesh points from 0 to 20 fm.

The training data of kinetic energies and densities are prepared by solving the Schrödinger equation with a mean potential for noninteracting systems. A combined Gaussian potential (CGP) is proposed to simulate the mean potential for nuclei, which is similar to the well-known Woods-Saxon potential for medium and heavy nuclei, but is more flexible and proper for light ones. In the present work, a series of CGPs are generated to build the training, validation, and test sets of kinetic energies and densities with some physical constraints on the potential depth and the root-mean-square (rms) radius. The details can be seen in Ref. [34].

In Fig. 1, 30000 samples of the training density distributions and the corresponding kinetic energies for nuclei with the total nucleon number $A = 4, 16, \text{ and } 40$ (10000 ones for each nucleus) are depicted. The lines give the density distributions and the colors represent the kinetic energies. While the training kinetic energies range from several tens MeV to more than one thousand MeV for different systems, the kinetic energies per nucleon are roughly several tens MeV, which is quite reasonable for most nuclei. The density distributions

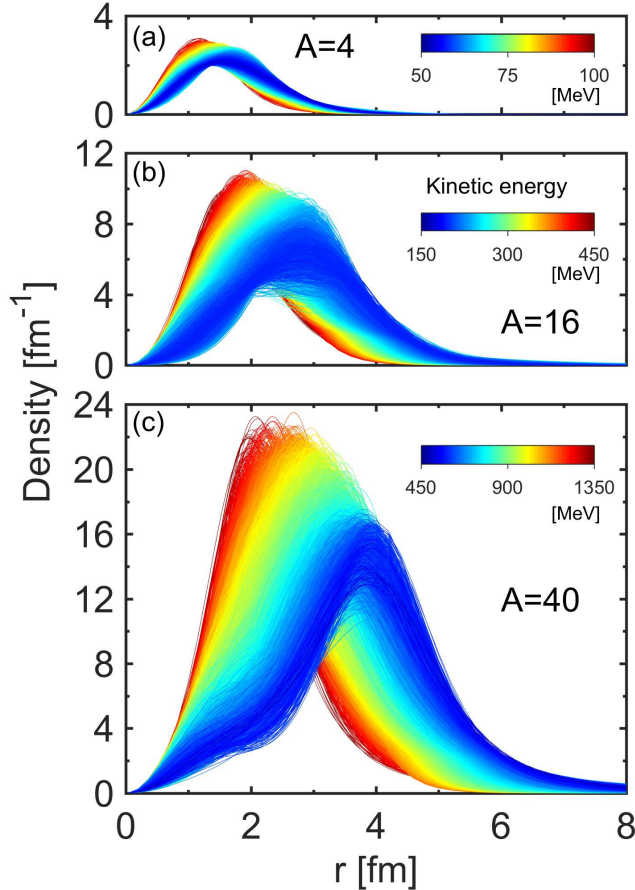


FIG. 1. (Color online). Training density distributions and the corresponding kinetic energies (color map) for nuclei with the total nucleon number $A = 4$ (top), 16 (middle), and 40 (bottom).

are closely related to the magnitudes of the kinetic energies according to the uncertainty principle, i.e., the tighter the density distribution, the higher the kinetic energy.

These 30000 training energy-density data are used to train the KRR network (3), and the solution can be obtained via Eq. (6). Here, the hyperparameters λ and σ are determined by optimizing the ML performance on the validation set containing 3000 samples of data (1000 ones for each nucleus). The resultant hyperparameters are $\lambda = 4.5 \times 10^{-13}$ and $\sigma = 0.66 \text{ fm}^{-1}$. Finally, a test set containing 3000 samples of data is used to provide an unbiased evaluation of the KRR learning on the training dataset.

In Fig. 2, the performance of the KRR functional is illustrated with the statistical histogram of the deviations ΔE_{kin} between the KRR predicted kinetic energies and the exact ones in the validation and test sets. It is seen that the KRR predictions nicely reproduce the kinetic energies in both validation and test sets and, in most cases, the deviations are

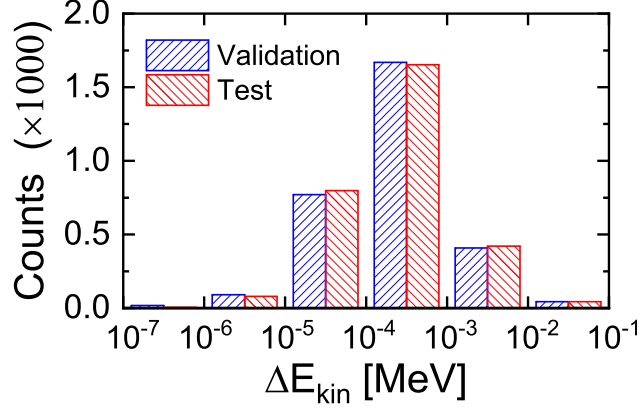


FIG. 2. (Color online). Statistical histogram of the deviations ΔE_{kin} between the KRR predicted kinetic energies and the exact ones in the validation and test sets.

below 1 keV, which is a very high accuracy for nuclear physics. More importantly, the count distributions of the deviations ΔE_{kin} are very similar for the validation and test sets. This means that the performances of the present high-accuracy KRR functional are equally well for the two datasets and, thus, the functional is very good in its generalization ability.

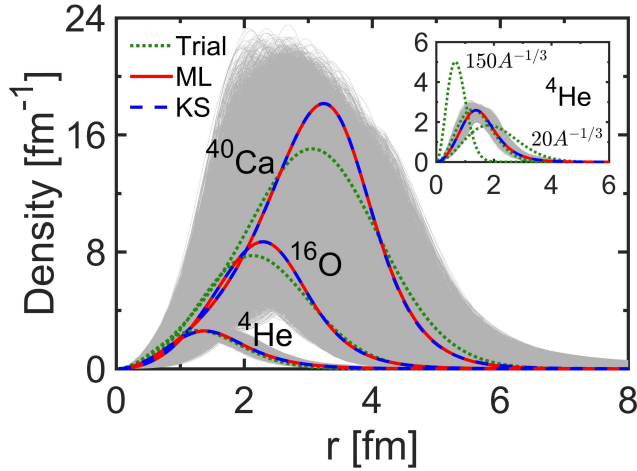


FIG. 3. (Color online). The trial (dotted lines) and self-consistent densities (solid lines) from the machine learning approach in comparison with the self-consistent densities obtained with the Kohn-Sham method (dashed lines) for ${}^4\text{He}$, ${}^{16}\text{O}$, and ${}^{40}\text{Ca}$. The shaded region shows the extent of variation of the training densities. The inset zooms in the densities for ${}^4\text{He}$ with two additional trial densities (see text).

While the ML functional predicts the energy in a very high accuracy, for orbital-free DFT,

one has to finally test the self-consistent procedures to find the density that minimizes the total energy. The iteration starts from a trial density which is intuitively taken as the empirical nuclear density in a harmonic oscillator (HO) potential with $\hbar\omega = 41 \cdot A^{-1/3}$ MeV [5].

In Fig. 3, the trial densities and the obtained self-consistent ones are depicted in comparison with the Kohn-Sham ground-state densities for ${}^4\text{He}$, ${}^{16}\text{O}$, and ${}^{40}\text{Ca}$. One can see that for all the three nuclei, the ground-state densities obtained with the present ML approach are in a very nice agreement with the Kohn-Sham ones. This clearly demonstrates that the success of the present ML density functional for nuclei. One may doubt that the trial densities here are coincidentally too close to the self-consistent ones. However, as seen in the inset of Fig. 3, for ${}^4\text{He}$, the trial density can actually be widely changed by tuning the HO strengths $\hbar\omega$ from $20 \cdot A^{-1/3}$ MeV to $150 \cdot A^{-1/3}$ MeV. It is surprisingly found that even if the trial density is out of the training data region, the convergence is still stable and accurate. The same conclusion holds true for ${}^{16}\text{O}$ and ${}^{40}\text{Ca}$ as well. Therefore, one can conclude that the performance of the present ML density functional in finding self-consistent densities is quite robust.

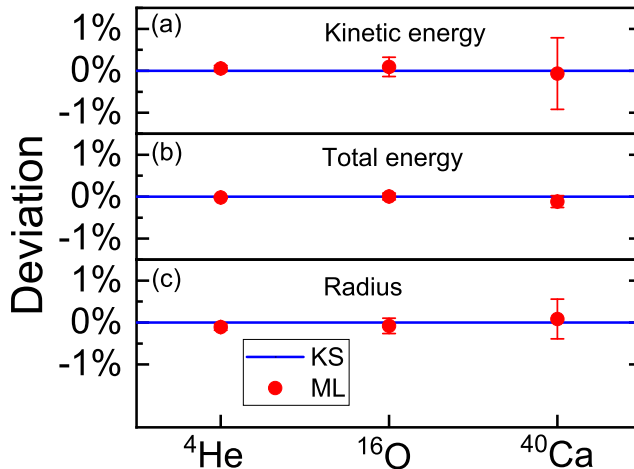


FIG. 4. (Color online). Relative deviations from the Kohn-Sham kinetic energies, total energies, and the root-mean-square (rms) radii for nuclei ${}^4\text{He}$, ${}^{16}\text{O}$, and ${}^{40}\text{Ca}$.

To qualitatively evaluate the influence of the trial density on the self-consistent results, we generate 100 trial densities by randomly sampling the HO strengths $\hbar\omega$ between $20 \cdot A^{-1/3}$ MeV and $150 \cdot A^{-1/3}$ MeV for nuclei ${}^4\text{He}$, ${}^{16}\text{O}$, and ${}^{40}\text{Ca}$, respectively. Starting from these trial densities, the self-consistent iteration produces a range of similar ground-state densities

and energies. Thus, the mean and standard deviation are taken as the final result and the corresponding uncertainty, respectively. The obtained self-consistent kinetic energies, total energies, and the rms radii are compared with the Kohn-Sham results in Fig. 4, where the relative deviations are presented. One can see that the central values of the present ML results agree nicely with the Kohn-Sham ones within a rather small deviation below 0.1% for all nuclei. Though the uncertainties are varying for different physical quantities and nuclei, we still reach a quite high accuracy. No existing orbital-free DFT comes close to this performance for nuclei. The uncertainties for the total energies are smaller than those for the kinetic energies and radii. This is due to the fact that nuclei are self-bound systems with short-range repulsive and long-range attractive nucleon-nucleon interactions. As a result, the kinetic and the interaction energies are elegantly balanced with the variation of the density around the equilibrium.

The uncertainties for ^{40}Ca are significantly larger than the other two nuclei. As seen in Fig. 1, the training data for $A = 40$ are more loosely distributed than those for $A = 4$ and $A = 16$, though the numbers of the training data are the same. This means that the training data are relatively sparse in the “energy-density” functional space for ^{40}Ca . Therefore, the uncertainties for ^{40}Ca can be simply reduced by increasing the training data or more efficiently improving their quality, i.e., including more data close to the self-consistent result.

The present study is the headmost work to build nuclear energy density functional from ML, and it aims for a proof of principle that ML approach can be successfully employed to build nuclear orbital-free DFTs with high precisions. For this purpose, only three nuclei are considered. However, it has been checked that the extrapolation ability of the present ML density functional to systems with other mass numbers is quite robust. Therefore, it is promising to extend the present ML functional to the whole nuclear chart. A detailed discussion can be found in Ref. [35]. Note that the computational complexity of the present KRR approach grows fast with the increase of the training set. Alternative ML approaches like neural network may be employed in the future, and some learning techniques (e.g., minibatch learning) can help to optimize the learning procedure.

In summary, for the first time, machine learning has been used to build an energy density functional for self-bound nuclear systems. The kernel ridge regression is employed to learn the kinetic energy as a functional of the nucleon density alone, and together with the interaction energy, it provides a robust and accurate orbital-free density functional for nuclei.

Self-consistent calculations have been carried out for ^4He , ^{16}O , and ^{40}Ca without solving the Kohn-Sham equations, and the obtained ground-state properties have been compared with the Kohn-Sham results. It is found that the obtained self-consistent densities, energies, and radii for the ground states agree quite well with the Kohn-Sham ones. The relative deviations are below 0.1% for all nuclei, and the uncertainties associated with varying trial densities have been analyzed quantitatively. It is found that the performance of the present ML density functional in finding self-consistent densities is quite robust and accurate. No existing orbital-free DFT comes close to this performance for nuclei. Therefore, it provides a new promising way for future developments of nuclear energy density functionals.

The pairing correlations could also be included in the present ML approach straightforwardly by treating the kinetic energy as a functional of normal and pairing densities. This would massively reduce the complexity of three-dimensional (3D) large-scale DFT calculations for nuclei by bypassing the 3D Hartree-Fock-Bogoliubov equation which is extremely expensive in computation for heavy nuclei. Besides the ground states of nuclei, the orbital-free DFT is also applicable for excited states. In fact, the time-dependent orbital-free DFT has been developed and applied to quantum many-body problems in many other fields, see e.g., Refs. [36–38]. It has shown a quite higher efficiency compared with the conventional time-dependent Kohn-Sham DFT calculations, which are rather time-consuming for nuclear many-body problems [39]. Therefore, the present machine-learning approach provides a promising way to develop time-dependent orbital-free DFTs for nuclear systems, which will be beneficial for solving the complex nuclear dynamical problems, such as fission and fusion problems.

This work was partly supported by the National Key R&D Program of China (Contracts No. 2018YFA0404400 and No. 2017YFE0116700), the National Natural Science Foundation of China (Grants No. 11875075, No. 11935003, No. 11975031, and No. 12070131001), and the China Postdoctoral Science Foundation under Grant No. 2020M670013.

* pwzhao@pku.edu.cn

[1] P. Hohenberg and W. Kohn, *Phys. Rev.* **136**, B864 (1964).

[2] W. Kohn and L. J. Sham, *Phys. Rev.* **140**, A1133 (1965).

- [3] S. Kümmel and L. Kronik, *Rev. Mod. Phys.* **80**, 3 (2008).
- [4] J. A. Maruhn, P.-G. Reinhard, and E. Suraud, *Simple Models of Many-Fermion Systems* (Springer-Verlag Berlin Heidelberg, 2010).
- [5] P. Ring and P. Schuck, *The nuclear many-body problem* (Springer-Verlag, New York, 1980).
- [6] M. Centelles, P. Schuck, and X. Viñas, *Ann. Phys.* **322**, 363 (2007).
- [7] M. Bender, P.-H. Heenen, and P.-G. Reinhard, *Rev. Mod. Phys.* **75**, 121 (2003).
- [8] D. Vretenar, A. V. Afanasjev, G. A. Lalazissis, and P. Ring, *Phys. Rep.* **409**, 101 (2005).
- [9] J. Meng, H. Toki, S. Zhou, S. Zhang, W. Long, and L. Geng, *Prog. Part. Nucl. Phys.* **57**, 470 (2006).
- [10] T. Nakatsukasa, K. Matsuyanagi, M. Matsuo, and K. Yabana, *Rev. Mod. Phys.* **88**, 045004 (2016).
- [11] G. Carleo, I. Cirac, K. Cranmer, L. Daudet, M. Schuld, N. Tishby, L. Vogt-Maranto, and L. Zdeborová, *Rev. Mod. Phys.* **91**, 045002 (2019).
- [12] G. Carleo and M. Troyer, *Science* **355**, 602 (2017).
- [13] J. C. Snyder, M. Rupp, K. Hansen, K.-R. Müller, and K. Burke, *Phys. Rev. Lett.* **108**, 253002 (2012).
- [14] F. Brockherde, L. Vogt, L. Li, M. E. Tuckerman, K. Burke, and K.-R. Müller, *Nat. Commun.* **8**, 872 (2016).
- [15] M. Bogojeski, L. Vogt-Maranto, M. E. Tuckerman, K.-R. Müller, and K. Burke, *Nat. Commun.* **11**, 5223 (2020).
- [16] S. Gazula, J. Clark, and H. Bohr, *Nucl. Phys. A* **540**, 1 (1992).
- [17] K. Gernoth, J. Clark, J. Prater, and H. Bohr, *Phys. Lett. B* **300**, 1 (1993).
- [18] R. Utama, J. Piekarewicz, and H. B. Prosper, *Phys. Rev. C* **93**, 014311 (2016).
- [19] L. Neufcourt, Y. Cao, W. Nazarewicz, E. Olsen, and F. Viens, *Phys. Rev. Lett.* **122**, 062502 (2019).
- [20] Z. Niu and H. Liang, *Phys. Lett. B* **778**, 48 (2018).
- [21] X. H. Wu and P. W. Zhao, *Phys. Rev. C* **101**, 051301(R) (2020).
- [22] L. Neufcourt, Y. Cao, W. Nazarewicz, and F. Viens, *Phys. Rev. C* **98**, 034318 (2018).
- [23] R. Utama, W.-C. Chen, and J. Piekarewicz, *J. Phys. G* **43**, 114002 (2016).
- [24] Y. Ma, C. Su, J. Liu, Z. Ren, C. Xu, and Y. Gao, *Phys. Rev. C* **101**, 014304 (2020).
- [25] D. Wu, C. L. Bai, H. Sagawa, and H. Q. Zhang, *Phys. Rev. C* **102**, 054323 (2020).

- [26] R.-D. Lasserri, D. Regnier, J.-P. Ebran, and A. Penon, *Phys. Rev. Lett.* **124**, 162502 (2020).
- [27] Z.-A. Wang, J. Pei, Y. Liu, and Y. Qiang, *Phys. Rev. Lett.* **123**, 122501 (2019).
- [28] J. Keeble and A. Rios, *Phys. Lett. B* **809**, 135743 (2020).
- [29] J. Shawe-Taylor and N. Cristianini, *Kernel Methods for Pattern Analysis* (Cambridge University Press, USA, 2004).
- [30] C. Saunders, A. Gammerman, and V. Vovk, in *Proceedings of the Fifteenth International Conference on Machine Learning, ICML1998* (Morgan Kaufmann Publishers Inc., San Francisco, CA, USA, 1998) pp. 515–521.
- [31] R. Y. Cusson, R. K. Smith, and J. A. Maruhn, *Phys. Rev. Lett.* **36**, 1166 (1976).
- [32] J. C. Snyder, M. Rupp, K.-R. Müller, and K. Burke, *Int. J. Quantum Chem.* **115**, 1102 (2015).
- [33] H. Abdi and L. J. Williams, *WIREs Computational Statistics* **2**, 433 (2010).
- [34] See Supplementary Material for information necessary to construct the machine learning data sets.
- [35] See Supplementary Material for illustration of extrapolation ability of the machine-learning approach.
- [36] A. Doms, P.-G. Reinhard, and E. Suraud, *Phys. Rev. Lett.* **80**, 5520 (1998).
- [37] Y. H. Ding, A. J. White, S. X. Hu, O. Certik, and L. A. Collins, *Phys. Rev. Lett.* **121**, 145001 (2018).
- [38] C. Covington, J. Malave, and K. Varga, *Phys. Rev. B* **103**, 075119 (2021).
- [39] Y. Hashimoto and G. Scamps, *Phys. Rev. C* **94**, 014610 (2016).